Hammett Structural Relationships Revealed in Chalcogen Bonded Co-crystals of Electron Rich Pyridines with 4′-Substituted Ebselen Derivatives

Thomas Fellowes,*,†,§ Eric Lee,‡ Jennifer Tran,‡ Ruyi Xu,† Alec Barber,† Samuel C. Brydon,† Jack K. Clegg,¶ and Jonathan M. White*,†

†*School of Chemistry and Bio21 Institute, The University of Melbourne, Parkville 3010, Australia*

‡*Penleigh and Essendon Grammar School, Rachelle Road, Keilor East 3033, Australia*

¶*School of Chemistry and Molecular Biosciences, University of Queensland, St Lucia 4072, Australia*

§*Current address: Department of Chemistry and Leverhulme Research Centre for Functional Materials Design, Materials Innovation Factory, University of Liverpool, 51 Oxford Street, Liverpool, L7 3NY, UK*

E-mail: thomas.fellowes@liverpool.ac.uk; whitejm@unimelb.edu.au

Abstract

In this work, a detailed Hammett structure-structure correlation was applied to a range of chalcogen bonded co-crystals prepared by combining 4′-substituted derivatives of the selenium-based drug ebselen with three different 4-amino-substituted pyridine based chalcogen bond acceptors of differing basicities. This established that the N···Se chalcogen bond distance is well within the sum of the van der Waals radii of Se and N and is sensitive to the electronic nature of the substituent. Thus N···Se distances ranging from 2.2424(5)–2.4496(9) Å were observed with the shorter distances being observed in co-crystals of ebselen substituted with

electron withdrawing groups. Associated with trends of the N···Se distance as a function of the 4′-substituent was lengthening of the internal Se−N bond distance consistent with a significant covalent contribution to N···Se chalcogen bonding in these derivatives. We define a covalency quotient for the chalcogen bond as the negative slope of the plot of the internal Se−N bond distance *vs* the external N···Se chalcogen bond distance. A value of 0.31 was obtained implying a significant covalent contribution to N···Se chalcogen bond. A similar result was obtained by an analysis of chalcogen bonded selenium containing molecules harvested from the Cambridge Crystallographic Database. The covalency quotient is extended to the general case for σ-hole interactions including halogen bonding and hydrogen bonding, and we show that the covalent component of such interactions can be inferred from the lengthening of the donor bond. The degree of charge transfer in a smaller number of chalcogen bonded co-crystals of ebselen was established by measuring experimental electron density using high-resolution x-ray diffraction to more accurately measure the degree of electron transfer and hence covalency. This showed that in the most strongly bound systems, up to 1 electron worth of charge is transferred from the Lewis base to the Ch-bond donor, which again clearly points to significant covalent character.

Introduction

Chalcogen bonding is an attractive non-covalent interaction involving a Lewis basic species and a molecule containing a polarised chalcogen atom (generally S, Se or Te bonded to an electronegative substituent, X).[1,2] It has found applications in many areas of chemistry, including medicinal chemistry,[3–7] materials chemistry,[8,9] catalysis,[10,11] anion sensing,[12–15] and supramolecular chemistry.[16–19] Chalcogen bonding has both orbital interaction and electrostatic components. The former involves charge transfer from the Lewis base non-bonded pair of electrons to an energetically accessible $\sigma^\star$ orbital on the chalcogen, while the electrostatic component involves the attraction between the Lewis base and the positively charged σ-hole, which is generated along the extension of the Ch-X bond due to polarisation of the chalcogen's electron cloud.[20–22] This latter interaction

is believed to dominate in the closely related phenomenon of halogen bonding.[23–28]

Ebselen **1**, which mimics the activity of glutathione peroxidase,[29] contains a benzisoselenazolinone ring system, which is a particularly effective chalcogen bond donor due to the polarised Se−N(CO) moiety. Chalcogen bonding dominates the crystal packing of **1**, which is characterised by a very short C=O · · · Se contact of 2.522(2) Å (sum of Van der Waals radii for O and Se = 3.42 Å) with the C=O oxygen closely aligned with the Se−N(CO) bond ($\angle$(O · · · Se−N) = 169.80(9)°). Topological analysis of the charge density obtained from high resolution x-ray crystallography data from **1** shows a bond critical point for the O · · · Se chalcogen bond with relatively low electron density and a positive Laplacian, consistent with an interaction which is substantially electrostatic in character.[30]

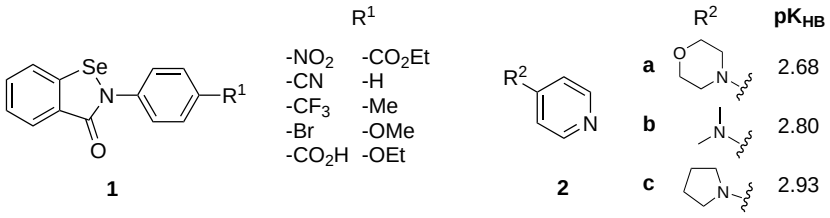

Figure 1: Structures of compounds used in this work.

Ebselen and its analogues form chalcogen bonded co-crystals with a variety of nitrogen bases including pyridine, 4-dimethylaminopyridine (DMAP), quinuclidine, and 1,4-diazabicyclo[2.2.2]-octane (DABCO), which are characterised by N · · · Se distances ranging from 2.304(1) Å to 2.6166(15) Å depending on the nature of the Lewis base and the substituted benzisoselenazolinone.[21,31] In this paper we report a systematic structural investigation on the electronic effect of the remote 4′-substituent on co-crystals formed between a range of ebselen derivatives **1R** and the three pyridine bases 4-morpholinylpyridine **2a**, 4-dimethylaminopyridine (DMAP) **2b**, and 4-pyrrolidinylpyridine **2c** (fig. 1) on the strength of the chalcogen bond as assessed by the N_{base} · · · Se and Se−N(CO) distances.

Results and discussion

Our previous work has shown that electron-rich pyridines (specifically DMAP) formed the strongest Ch-bonds out of all the bases trialled,[21] consistent with the hydrogen bond basicity (pK_{HB}) of the bases.[32] The planar geometry and aromatic character of DMAP may also facilitate crystallisation, as opposed to the relatively bulky aliphatic bases, which do not crystallise as reliably. For these reasons, we restricted the bases used in this study to other electron-rich pyridines.

Although DMAP **2b** is already a very strong base, the basicity can be increased further by incorporating the aniline-like nitrogen into an aliphatic ring. This reduces the energetic penalty associated with the delocalisation of the lone pair into the pyridine ring by forcing a more planar geometry upon the nitrogen.[32,33] Compounds **2a** and **2c** were therefore synthesised by treating 4-chloropyridine hydrochloride with 2 equivalents of the appropriate base (scheme S1). **2c** is a stronger base due to the imposed planarity of the aniline nitrogen, while **2a** is weaker due to the larger ring and inductively electron withdrawing oxygen atom.

The benzisoselenazolinone derivatives **1R** were prepared by the reaction of substituted anilines with the dichloride **3**, which is ultimately derived from anthranilic acid (scheme S2). Co-crystals of the benzisoselenazolinones and pyridines were grown by vapour diffusion from an equimolar solution in dichloromethane/pentane.

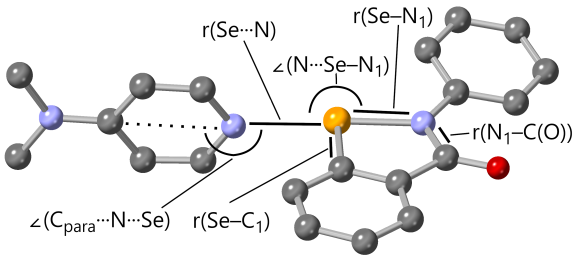

Figure 2: Depiction of relevant geometric parameters in **1R**·pyridine co-crystals.

We begin by analysing trends in the co-crystals with the weaker and stronger bases **2a** and **2c** respectively. A number of structural parameters are of particular relevance in this investigation, which are shown in fig. 2. Of primary importance is the Ch-bond distance r(N · · · Se), which serves as an indicator of the strength of the interaction. In all cases, this distance is well within the sum of

the van der Waals radii of selenium and nitrogen (3.42 Å), with distances ranging from 2.2424(5) Å to 2.4496(9) Å, which is indicative of a strong N $\cdots$ Se interaction.

Another important parameter is the endocyclic Se−N bond length r(Se−N_1), which is sensitive to the occupancy of the $\sigma^\star$(Se−N_1) antibonding orbital. Higher occupancies will lead to weakening and hence lengthening of the bond, which can then be related to the covalent or electron-sharing character of the Ch-bonding interaction due to the n(N) $\rightarrow$ $\sigma^\star$(Se−N_1) orbital overlap. For comparison, the endocyclic Se−C bond length r(Se−C_1) is also presented as a control. Any isotropic effects at the selenium would be expected to alter the r(Se−N_1) and r(Se−C_1) bond lengths equally, so the strong directionality of the Ch-bond can be inferred from the selective lengthening of the former.

Another parameter of potential interest is the amidic N−C distance r(N_1−C(O)). This bond length (and the carbonyl C=O bond length) may be sensitive to charge transfer from the pyridyl nitrogen, through the selenium, onto the carbonyl oxygen as represented by the charge-separated structure (fig. S1). As the degree of charge separation becomes greater, r(N_1−C(O)) is expected to decrease due to increased double bond character. Similarly, r(C=O) is expected to increase as it adopts more enolic bond character.

As mentioned above, σ-hole interactions are characterised by their strong directionality and so we present the angles subtended by:

a) the Lewis basic atom, the selenium atom, and the amidic nitrogen $\angle$(N $\cdots$ Se − N_1), and

b) the lone pair on the Lewis base, estimated as the angle described by the selenium atom, the Lewis basic atom, and the *para* carbon of the pyridine ring $\angle$(C_{para} $\cdots$ N $\cdots$ Se).

In all cases these angles would be expected to be close to 180°, in order to maximise n(N) $\rightarrow$ $\sigma^\star$(Se−N_1) orbital overlap. Any deviations may be attributed to crystal packing forces disrupting the ideal geometry, and this should be reflected in the parameters which are sensitive to the antibonding orbital occupancy (r(Se−N_1) and r(N_1−C(O))). A parameter which encompasses both these angles ψ has been defined for X-bonds, such that for a perfectly aligned X-bond where $\angle$(A $\cdots$ X − D) = $\angle$(X $\cdots$ $A_{lone\ pair}$) = 180° ψ is equal to 1, and as either angle approaches 90° ψ

tends to 0.[34] As this can be directly translated to Ch-bonding, we present values of ψ for these co-crystals.

The endocyclic bond lengths r(Se−N_1) of the free (not coordinated to a pyridine base) organoselenium derivatives were first inspected. These data, shown in table S1 and fig. S2, display little dependence on the electronic properties of the aryl group. This is not unexpected given that these derivatives are not actually free, but exist within a crystal which, in all cases, consists of linear chains of molecules Ch-bonded through the carbonyl oxygen. The basicity of this oxygen atom is likely to be strongly influenced by the electron demand of the aryl group. As the magnitude of the σ-hole (Ch-bond donor ability) is *increased* by an electron withdrawing substituent, the Ch-bond acceptor ability of the carbonyl is *decreased*. These opposing effects, which appear to be approximately equal in magnitude, cancel each other out and the result is a very flat and featureless Hammett plot (fig. S2).

However, inspection of the same bond length (see table S2) in co-crystals of ebselen derivatives and a Lewis base results in a much clearer dependence, as can be seen in fig. 3. This is because the Ch-bond acceptor ability is now independent of the electronic properties of the Ch-bond donor and so the endocyclic r(Se−N_1) bond length is determined solely by the latter. An inverse correlation can be seen in the r(Se$\cdots$N) Ch-bond length.

These trends demonstrate the expected relationship between Ch-bond length and electron demand of the donor. As the chalcogen atom becomes less electron rich, it can interact more strongly with a Lewis base, leading to a shorter Ch-bond distance. The shorter bond distance leads to more effective n(N) $\rightarrow \sigma^{\star}$(Se−$N_1$) orbital overlap, causing increase occupation of the antibonding orbital and lengthening of the r(Se−N_1) bond length.

There is a difference in the slopes of the two Hammett plots presented so far (**2a** *vs* **2c** in fig. 3). The parameters describing the lines are shown in table 1, in which we see a qualitative link between the strength of the base used and the gradient of the line of best fit. The Ch-bond length in co-crystals with the weaker base **2a** depends *more* strongly on the electronic properties of the aryl group than in co-crystals with the stronger base **2c** (gradient = −0.15(3) Å *vs* −0.07(1) Å). **1Me**·**2c** is clearly an

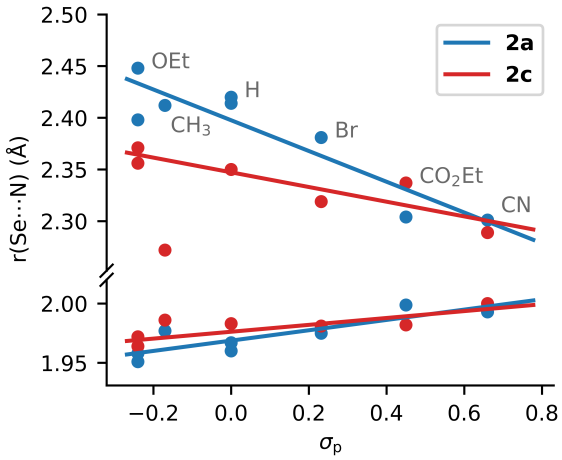

Figure 3: Hammett plots of endocyclic r(Se−N_1) bond length and r(Se···N) Ch-bond length of ebselen derivatives complexed with **2a** and **2c** against substituent parameter σ_p. The upper lines represent the r(Se···N) Ch-bond distance, and the lower lines represent the endocyclic r(Se−N_1) bond length (see table 1 for linear regression results).

outlier, which may be attributed to enhancement of the Ch-bond donor ability by non-conventional H-bonding to the carbonyl oxygen of the donor. This interaction is absent in other structures. We have previously reported this phenomenon in similar systems, although the C−H H-bond donor is substantially weaker than previously observed.[21] This point is retained in the plot for the sake of completeness, but was not used in the linear regression.

Table 1: Linear regression results for Hammett plots in figs. 3 and 4.

Base	pK_{HB} [32]	r(Se···N)			r(Se−N_1)		
		gradient	intercept	R^2	gradient	intercept	R^2
2a	2.68	−0.15(3)	2.398(9)	0.8354	0.04(1)	1.968(3)	0.7389
2b	2.80	−0.12(4)	2.36(2)	0.4104	0.07(1)	1.959(4)	0.7857
2c	2.93	−0.07(1)	2.347(7)	0.8005	0.029(7)	1.976(2)	0.7828

Now we will consider the structural parameters of the co-crystals with **2b**, whose basicity is approximately halfway in between that of **2a** and **2c**. We were fortunate to obtain high quality co-crystals of a wider variety of derivatives with **2b**, which revealed an interesting phenomenon. Although the same trend is seen for both r(Se−N_1) and r(Se···N) as in co-crystals with **2a** and **2c** (insofar as increased electron demand of the aryl group leads to a longer r(Se−N_1) and shorter

r(Se···N)), we also observe significant scatter for the electron rich derivatives on the left hand side of the plot (fig. 4). While the more strongly Ch-bonded systems (with electron withdrawing substituents) are well described by the model, complexes containing the electron rich derivatives **1OMe** and **1OEt** vary significantly in their N···Se Ch-bond distances. Indeed, in the case of **2b** complexes, omitting these data points improves the R^2 value to 0.8148 from 0.4104 while the gradient and intercept are almost unchanged at −0.15(3) Å and 2.38(2) Å respectively. Both **1OMe** and **1OEt** contain more than one Ch-bonded system in the asymmetric unit, and two distinct polymorphs were isolated in the case of **1OMe** by vapour diffusion of pentane into diethyl ether as opposed to dichloromethane. We believe it is unlikely to be a coincidence that only the electron rich derivatives display such variation in Ch-bond lengths.[35] In the same way that the Ch-bond is more easily distorted when a weaker base is used (fig. 3), the geometry can be more easily disrupted by crystal packing forces when weaker (more electron rich) Ch-bond donors are used, leading to polymorphism and multiple molecules in the asymmetric unit.[36]

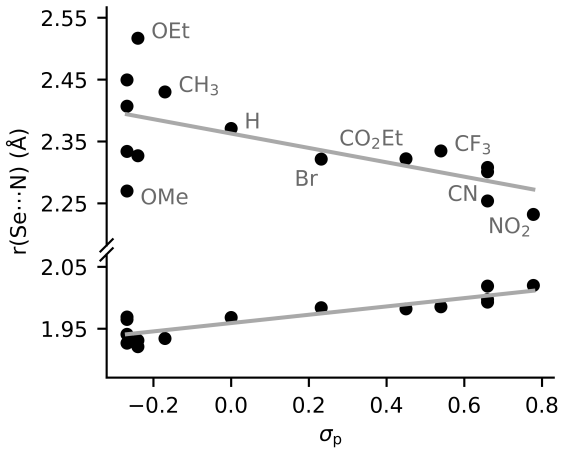

Figure 4: Hammett plots of endocyclic r(Se−N_1) bond length and r(Se···N) Ch-bond length of ebselen derivatives complexed with **2b** against substituent parameter σ_p.

The linearity parameter ψ could reasonably be expected to respond to the electron demand of the substituent, insofar as a more electron withdrawing group will give rise to a stronger Ch-bond, which may be more linear. A weak correlation can be seen in fig. 5.

The amidic bond length r(N_1−C(O)) displays only a slight variation with the electronic character

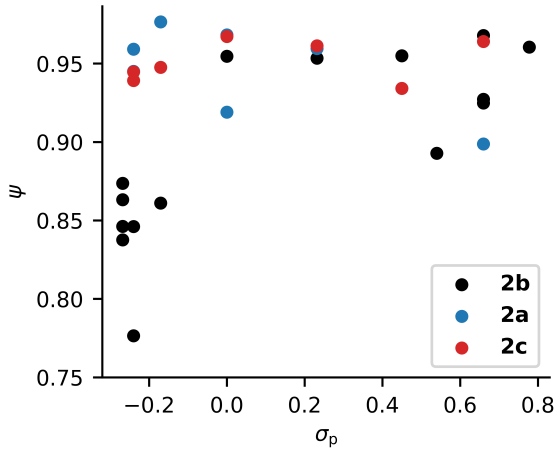

Figure 5: Hammett plot of linearity parameter ψ for ebselen derivatives complexed with all bases against substituent parameter σ_{p}.

of the system, as can be seen in fig. S3. This indicates that any delocalisation of the charge from the Lewis base onto the carbonyl has a minimal structural effect (as in fig. S1), and that accumulation of negative charge (if any) likely occurs at the nitrogen N_1.

The diversity in Ch-bond environments in the systems we have presented provides the opportunity to estimate the covalent (as opposed to electrostatic and dispersive) character of the Ch-bond. We examine the change in r(Se–N_1) endocyclic bond length compared to the Ch-bond distance r(Se $\cdots$ N), by plotting r(Se–N_1) against r(Se $\cdots$ N) as in fig. 6.

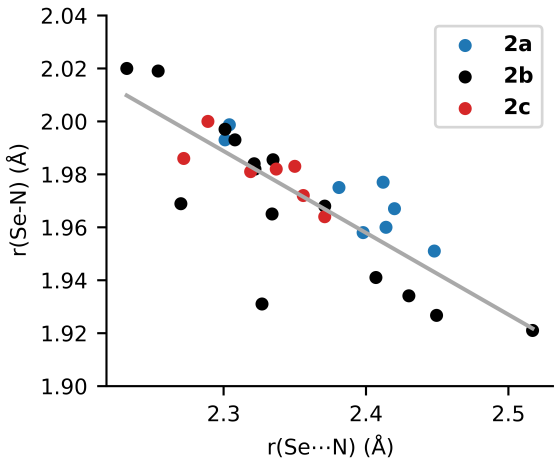

Figure 6: Estimation of the covalency quotient for **1R**·pyridine Ch-bonds, by plotting donor bond length against Ch-bond distance.

The gradient of this line is −0.31, indicating that for every unit change in Ch-bond length, the donor bond length changes by 0.31 units in the opposite direction. We have named the negative of this ratio the "covalency quotient", and we propose that it is a general and experimentally accessible estimate of the covalent character of a σ-hole interaction, encompassing not just Ch-bonds but halogen-, pnictogen-, tetrel-, and even hydrogen-bonds. The lower limit of 0 corresponds to an entirely electrostatic interaction, where there is no energetically accessible antibonding orbital whose partial filling leads to donor bond lengthening. Conversely, the upper limit of 1 corresponds to complete transfer of the acceptor electron pair to an antibonding orbital. Such a situation would be found when a ground state geometry is very close to an S_N2 transition state, or in formal 3-centre 4-electron bonding.

In naming this quantity the covalency quotient, we take a somewhat conservative definition of covalency in that we consider it to be the limiting case for a hyperconjugative interaction between an electron pair and a single antibonding orbital. We use this definition as our method relies on structural changes as a measure of Lewis-type orbital occupancy. Other definitions of covalency (e.g. Roby-Gould Bond Indices) take a more holistic view, and consider all sources of electron sharing.[37] However, this requires access to a wavefunction which is not directly observable. The key advantage of considering covalency as single hyperconjugative interaction is that the resulting structural changes are apparent even in comparatively low-quality crystal structures.

Over a small range of electronically similar systems such as the data presented above, a linear approximation is valid. However, this breaks down when considering more diverse systems, which gives a hyperbolic relationship between donor and acceptor bond length. This has been observed for more or less symmetric H-bonds, secondary bonds in bismuth chlorides, and trihalides among others.[38,39] We model this with an equation of the form

$$\mathrm{r(D{-}X)} = \mathrm{r(D{-}X)_0} + \frac{a}{\mathrm{r(X\cdots A)} - \mathrm{r(X\cdots A)_0}} \tag{1}$$

where $\mathrm{r(D{-}X)_0}$ and $\mathrm{r(X\cdots A)_0}$ are respectively the asymptotic donor and complex bond lengths,

and a is a parameter that measures the sensitivity of the donor bond length to the approach of the acceptor. Taking the gradient of this function by differentiation allows the determination of the covalency quotient for any complex in the series used to fit the data, simply as a function of the donor-acceptor distance. The covalency quotient therefore smoothly increases from zero at a large separation to a maximum value of one. The covalency quotient can of course be extrapolated to values beyond one (as long as the first derivative of the fitting function is finite), however such a situation would correspond to an inversion of the donor and acceptor moieties in the complex. Simply swapping the donor and acceptor bond lengths will afford a covalency quotient in the expected range of zero to one, and will correspond to the intuitive flow of electron density.

To show the validity of this method, we augmented our structural data with a broader range of Ch-bonded systems taken from the Cambridge Structural Database (CSD), in which a divalent selenium atom bonded to C, N, O or X (where X is a halogen) bears a close contact to a nitrogen or oxygen opposite the first group ($\angle(\mathrm{D{-}Se\cdots A}) > 170°$, 226 hits, fig. 7). In this case we analysed distances between disparate types of atoms, which would presumably have different "typical" bond lengths/vdW distances to the selenium atom. We therefore normalised all contacts and bond lengths simply by dividing by the sum of the vdW radii of the participating atoms, as has been previously done by Puttreddy *et al.*[40] This dimensionless quantity is referred to herein as a normalised distance $\mathrm{r}_n(\mathrm{X{-}Y}) = \mathrm{r(X{-}Y)}/(\mathrm{r_{vdW}(X) + r_{vdW}(Y)})$.

The co-crystals which we presented above (fig. 6) are found on the left hand side of fig. 7, with extremely short normalised distances of ~ 0.72. At this distance, the covalency quotient is 0.33, which agrees well with the linear fit of the same data. The covalency quotient smoothly decays to zero as the distance approaches the VdW limit.

We also examined a variety of other systems which show similar secondary bonding interactions.[41] Firstly, we considered halogen bonds (X-bonds) between 2,3,5,6-tetrafluoroiodobenzenes and nitrogen bases. A search of the Cambridge Structural Database (CSD) afforded 263 hits for an iodine-nitrogen close contact consistent with a X-bond, where the $\angle(\mathrm{C{-}I\cdots N})$ angle was within 5° of linearity. Plotting the r(C−I) distance against the $\mathrm{r(I\cdots N)}$ distance (fig. 8a) affords a fit which is markedly

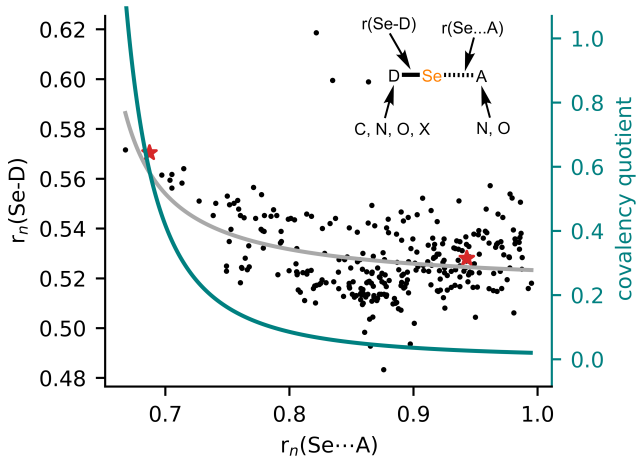

Figure 7: Ch-bond donor length *vs* Ch-bond distance, for the CSD query inset (226 results). The data are fit by the equation $\mathrm{r}_n(\mathrm{Se{-}D) = 0.52 + \frac{0.0027}{r_n(Se\cdots A)-0.63}}$.

flatter than that of the Ch-bonded systems presented earlier in this work. For all structures, the covalency quotient is less than 0.15. This suggests that there is less effective n(N) $\rightarrow \sigma^{\star}$(I–C) orbital overlap, and that this type of X-bonding has little covalent character. This is in line with conclusions reached by other studies,[42–44] which suggest that polyfluoroiodobenzene-based X-bonds are predominantly electrostatic.

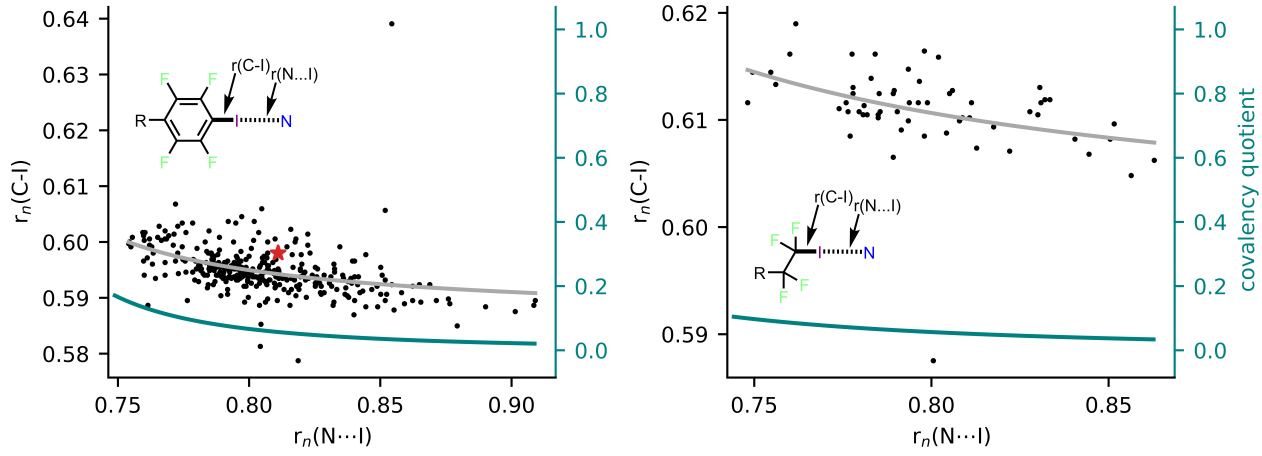

(a) (b)

Figure 8: X-bond donor length *vs* X-bond distance, for the CSD queries inset (263 and 54 results respectively). The data are fit by the equations $\mathrm{r}_n(\mathrm{C{-}I) = 0.586 + \frac{0.0011}{r_n(N\cdots I)-0.672}}$ and $\mathrm{r}_n(\mathrm{C{-}I) = 0.599 + \frac{0.0024}{r_n(N\cdots I)-0.598}}$.

A similar analysis of structures containing a N$\cdots$I close contact in structures with a 1,1,2,2-tetrafluoroiodoethane moiety ($\angle$(C$-$I$\cdots$N) > 175°, 54 hits) afforded a similar result with maximum covalency quotient of less than 0.14 (fig. 8b).

We also analyse H-bonding within this framework using the same criteria. Due to the difficulty in locating hydrogen atoms in x-ray diffraction data, we limited our search to structures which had been determined using neutron radiation. We note that this may introduce a bias in our results, as neutron diffraction is not a routine technique, and is mainly used to study systems which contain chemically "interesting" H-bonds. This subset is likely to consist of either extremely strong or weak H-bonds, and is therefore not representative of the whole gamut of interactions.

H-bonding (where the donor is an O-H group) displays a similar phenomenon to Ch-bonding, where there are distinct degrees of covalency (fig. 9). The shortest H-bonds (r_n(H$\cdots$A) < 0.4) had a large covalency quotient approaching unity, and this smoothly decays to zero. This is consistent with a similar analysis performed by Ceccarelli *et al.*, where a statistically significant inverse correlation between r(H$\cdots$O) and r(O$-$H) was observed in H-bonds in carbohydrates where r(H$\cdots$O) < 1.812 Å.[45] They note, however, that approximately half of this inverse correlation can be attributed to decreased librational shortening of the O$-$H bond length as the hydrogen becomes involved in a strong H-bond. Incorporating librational corrections for all of these structures was considered to be beyond the scope of this work, so we present the covalency quotients with the caveat that they are likely to be overestimated.

In order to further support our claim that the covalency quotient is a reliable indicator of the charge-transfer component of an interaction, we conducted an energy decomposition analysis on five model systems which represent X-bonding, and H- and Ch-bonding in strong and weak regimes. These systems are marked as red stars in figs. 7, 8a, 8b and 9, and the extracted complexes were reoptimised to a gas phase minimum.[46] The SAPT scheme was chosen due to its robust mathematical grounding and straightforward implementation.[47,48] The charge transfer energy in SAPT E_{CT} corresponds to the difference between the induction components E_{ind} (which quantifies redistribution of charge) calculated in the dimer basis and the monomer basis.[49] Further details

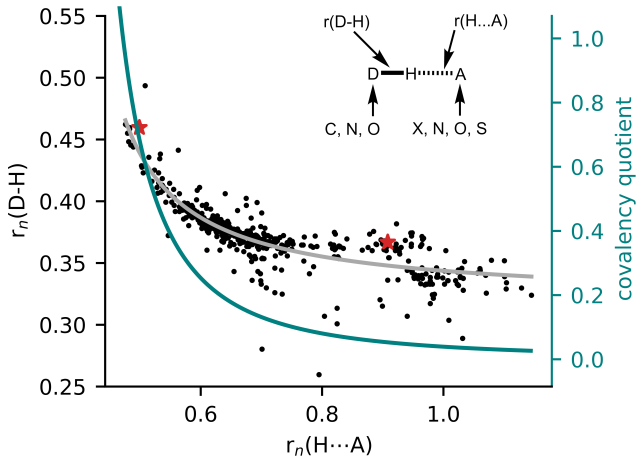

Figure 9: H-bond donor length *vs* H-bond distance, for the CSD query inset (neutron structures only, 249 results). The data are fit by the equations $r_n(O{-}H) = 0.319 + \frac{0.0157}{r_n(H{\cdots}A){-}0.369}$.

of the calculations are available in the Supporting Information (page S-11). The total interaction energy E_{tot}, charge transfer energy E_{CT}, ratio of the two, and covalency quotient as determined above are shown in table 2, and good qualitative agreement is observed, insofar as systems with a high covalency quotient have a more substantial charge transfer component as calculated by SAPT. We note that the E_{CT} component of the strong Ch-bond is extremely high, almost three times the total interaction energy. This may be due to n(Se) $\rightarrow \pi^{\star}$(pyridine) back-bonding which is not treated separately to the primary n(N) $\rightarrow \sigma^{\star}$(Se−N) delocalisation in the SAPT scheme. In principle such back-bonding is possible for the X-bonding case as well, though this is not evident in the SAPT analysis. In fact, the E_{CT} component for X-bonding is greater than zero, indicating a destabilising contribution to the total interaction energy.

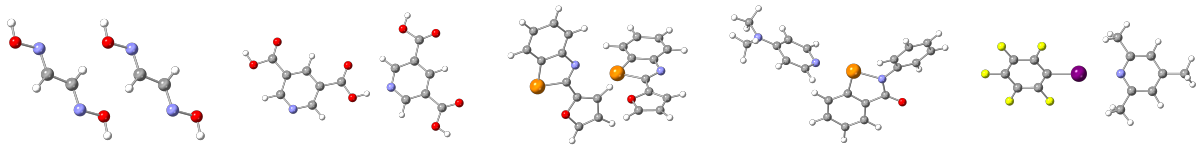

(a) Weak H-bond **GLOXIM11** (b) Strong H-bond **DINICA12** (c) Weak Ch-bond **OLUGEJ** (d) Strong Ch-bond **GOBYEE** (e) X-bond **LEZPIQ**

Figure 10: Model systems for SAPT analysis. Structures from which these were extracted are marked as stars in figs. 7, 8a, 8b and 9.

We note that some lengthening of the donor bond might plausibly be attributed to electrostatic

Table 2: SAPT results and covalency quotient for model systems shown in fig. 10.

Complex	E_{CT} kcal/mol	E_{tot} kcal/mol	E_{CT}/E_{tot}	Covalency quotient
H-bond (weak)	−0.11	−1.73	0.064	0.043
H-bond (strong)	−21.81	−34.89	0.63	0.88
Ch-bond (weak)	−1.79	−9.73	0.18	0.027
Ch-bond (strong)	−28.87	−10.54	2.74	0.81
X-bond	5.88	−9.69	−0.62	0.059

effects, in the sense that there exists an electrostatic attraction between the atoms in a highly polarised bond which is diminished as the charge is partially neutralised by the approach of the Lewis base, which may induce some lengthening of the bond. This is difficult to quantify, however we attempted to model this potential electrostatic lengthening using the NBO deletion method.[50] By zeroing all orbital overlap from one fragment to another, a geometry is obtained which can be entirely attributed to the electrostatic interaction energy. The difference between the bond distances with and without the deletion is denoted as Δ_{orb}, and the difference between the complex (without deletion) and the free donor is Δ_{tot}. Δ_{orb} contains *only* the lengthening due to orbital overlap, while Δ_{tot} contains the sum of orbital lengthening, and electrostatic lengthening. Geometry optimisation on a so-called deletion potential energy surface is extremely computationally costly, so we required simpler systems than those used for the SAPT analysis. These systems were intuitively chosen to be of similar Ch-/X-/H-bond strength to those studied above, and are shown in fig. 11. The results of this deletion analysis are presented in table 3. PBE0/6-31G(d,p) (with GD3 empirical dispersion) was used for this analysis (see Supporting Information page S-13 for further details).

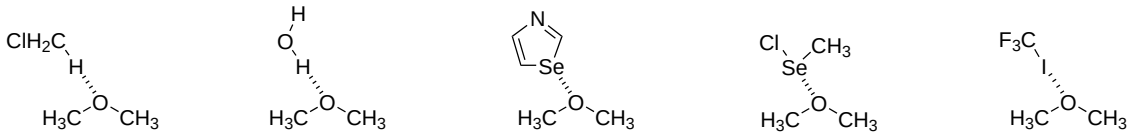

(a) Weak H-bond (b) Strong H-bond (c) Weak Ch-bond (d) Strong Ch-bond (e) X-bond

Figure 11: Model systems for NBO deletion analysis.

Several phenomena are evident in this data. Firstly, the most covalent systems according to

Table 3: NBO deletion analysis of model systems shown in fig. 11.

Complex	r(D···A)			r(X – D)				
	No deletion Å	Deletion Å	Δ	No deletion Å	Deletion Å	Free Å	Δ_{orb}	Δ_{tot}
H-bond (weak)	2.253	2.882	+28%	1.100	1.095	1.098	−0.5%	−0.2%
H-bond (strong)	1.923	2.698	+40%	0.983	0.970	0.973	−1.3%	−1.0%
Ch-bond (weak)	3.004	3.652	+22%	1.895	1.903	1.895	+0.3%	0%
Ch-bond (strong)	2.516	3.509	+40%	2.259	2.218	2.211	−1.8%	−2.1%
X-bond	2.944	3.720	+26%	2.235	2.239	2.242	+0.2%	+0.3%

SAPT (strong H-bond and strong Ch-bond) display a greater lengthening of the interaction distance r(D···A) as compared to the more electrostatic systems (40% compared to <28%). This reinforces the importance of orbital overlap in the strength of these interactions. Secondly, the total donor bond lengthening in all cases Δ_{tot} is of a similar magnitude to that attributable to the orbital overlap Δ_{orb} (±0.3 percentage points), indicating that electrostatic bond lengthening as suggested above is negligible. Thirdly, the weak Ch-bonded and X-bonded systems (which show little covalent character according to SAPT) display a paradoxical *contraction* of the donor bond in response to the approach of the acceptor. We note that in the former case, the covalency quotient is negative, and in the latter (as mentioned above) the charge-transfer energy E_{CT} is positive (repulsive) according to the SAPT calculations (table 2). These observations are all broadly consistent with an interaction which is predominantly electrostatic.

An alternative measure of covalency from experimental geometries has been proposed by Reed, Curtis and Weinhold, which was termed the covalency ratio χ.[51] This is calculated from the measured interaction distance, and from the covalent and van der Waals radii of the interacting atoms according to the equation $\chi = \frac{r_{vdW} - r_{eq}}{r_{vdW} - r_{cov}}$. Although this has the benefit of only requiring a single measurement (r_{eq}), the covalency ratio appears to draw a false distinction in covalent contribution between — for instance — strong and weak X-bonding (for which χ is equal to 56% and 29%, respectively). This is at odds to conclusions reached by various studies (as well as our own work) which indicate that both strong and weak X-bonding (in perfluoroiodoalkanes and arenes) are almost entirely electrostatic.[42–44] We therefore suggest that our covalency quotient is a useful addition

where more data is available, which is able to reveal differences (or the lack thereof) between different subclasses of interaction.

This first step towards a fully experimental energy decomposition analysis scheme led us to seek a method for estimating the electrostatic character of an interaction. Fortunately, the Quantum Theory of Atoms In Molecules (QTAIM) provides a convenient classification of interactions based on properties of the electron density at the bond critical point.[52] Although QTAIM is most often applied to electron densities derived from a wavefunction (calculated by DFT or wavefunction methods), the electron density in a crystal is an observable quantity that can be measured by x-ray diffraction experiments.

We turned back to our benzisoselenazolinone derivatives, as a number of the co-crystals studied above afforded data of sufficient quality that we were able to model the electron density *via* multipole refinement.[53] We were fortunate that these high-quality co-crystals spanned the range of electron demand (**1NO$_2$·2b** as the electron poor derivative, **1·2b** as a neutral derivative, and **1Me·2b** as an electron rich derivative), giving us the opportunity to examine differences in the experimental charge density in weakly and strongly bonded systems. We were also able to compare these co-crystals with previously reported charge-density studies of single component crystals of ebselen itself (**1**), and a *meta*-pyridyl derivative (**1Py**).[54,55] The BCPs in the vicinity of the selenium were first inspected, and the values of ρ_{BCP} and $\nabla^2\rho_{\mathrm{BCP}}$ for the Ch-bond (Se$\cdots$A) and endocyclic Se–N and Se–C bonds are given in table 4.

Table 4: QTAIM parameters of Ch-bonded complexes. ΔQ is given in terms of electrons transferred *from* the pyridyl moiety to the organoselenium species.

Complex	Se$\cdots$A		Se–N		Se–C		ΔQ
	ρ_{BCP} e·Å^{-3}	$\nabla^2\rho_{\mathrm{BCP}}$ e·Å^{-5}	ρ_{BCP} e·Å^{-3}	$\nabla^2\rho_{\mathrm{BCP}}$ e·Å^{-5}	ρ_{BCP} e·Å^{-3}	$\nabla^2\rho_{\mathrm{BCP}}$ e·Å^{-5}	QTAIM e
1NO$_2$·2b	0.560	1.970	0.808	1.567	1.086	−0.340	0.950
1·2b	0.391	1.539	0.826	2.210	1.093	−0.395	0.272
1Me·2b	0.330	2.596	0.930	3.094	1.086	−1.290	0.261
1[54]	0.251	2.452	0.940	3.200	1.030	0.500	—
1Py[55]	0.340	2.910	0.778	5.366	0.987	4.303	—

The electron density is concentrated in the covalent C−C bonds, but less so in the Ch-bond (figs. S5 to S7). This concentration, which is quantified by the Laplacian at the BCP $\nabla^2\rho_{\mathrm{BCP}}$, is characteristic of covalent bonds. More negative values of $\nabla^2\rho_{\mathrm{BCP}}$ correspond to more charge concentration, therefore a higher degree of covalency. The Laplacian at the Ch-bond BCP is positive, in contrast to the covalent bonds where it is negative. The substantially less polarised Se−C bond has a larger ρ_{BCP} value, and the Laplacian $\nabla^2\rho_{\mathrm{BCP}}$ is generally less than zero, which is expected for a covalent bond. In isolation, the positive value of $\nabla^2\rho_{\mathrm{BCP}}$ in the Ch-bond would suggest a predominantly electrostatic interaction, however we note that the endocyclic Se−N bond has similar values for $\nabla^2\rho_{\mathrm{BCP}}$ and ρ_{BCP}, suggesting that this bond has similar character to the $\mathrm{Se}\cdots\mathrm{N}_{\mathrm{pyridyl}}$ Ch-bond. This is therefore more reminiscent of a 3-centre–4-electron bond, as seen in strongly X-bonded systems such as trihalides.[56] Such bonding can be understood as the limiting case for charge-transfer complexes, thus underscoring the significance of the covalent energetic contribution in these complexes.

Perhaps more convincingly, the charge-transfer component of Ch-bonding can be directly extracted from the multipole model by integration of electron density corresponding to each fragment, and subtracting that which would be expected for exactly neutral molecules. A robust method of partitioning atoms and molecules is found in the QTAIM framework, in which QTAIM atoms are bounded by zero-flux surfaces of the electron density gradient. These QTAIM atoms are unique and transferrable, and integration of the electron density over these regions of space gives a meaningful estimate of atomic charge. The magnitude of charge-transfer between QTAIM molecules is presented in table 4 as $\Delta Q_{\mathrm{QTAIM}}$. Charge-transfer values are not presented for the single-component crystals, as it is not straightforward to separate each molecule into donor and acceptor fragments. For comparison, a variety of computational estimates of charge-transfer are also presented in table S5.

Conclusion

We have demonstrated that a Hammett relationship exists in Ch-bonded co-crystals of 4′-substituted ebselen derivatives and electron rich pyridines, in that increasing the electron demand of the Ch-bond donor decreases the resulting Ch-bond length. As part of this work, we observed the shortest Ch-bond identified to date, between the extremely electron deficient nitro derivative **1NO$_2$** and DMAP **2b**. A correlation was also found between the basicity of the Ch-bond acceptor (**2a**, **2b** and **2c**) and the slope of the Hammett relationship, with stronger bases giving a greater slope. Interestingly, significant scatter was observed for the strongly electron donating alkoxyl substituents where the N$\cdots$Se distances differed wildly between different polymorphs, or between different molecules when $Z' > 1$. We attributed this to the weaker and readily deformed N$\cdots$Se chalcogen bond for the electron rich alkoxyl substituents, making this parameter more susceptible to differing packing environments. This detailed structural characterisation also afforded us the opportunity to measure various other structural parameters, notably the r(Se$\cdots$N) bond length in the Ch-bond donor, which was found to be negatively correlated with the Ch-bond distance. We attribute this to partial filling of the $\sigma^\star$(Se$\cdots$N) antibonding orbital by the approaching lone pair of the Lewis base, indicating a partial covalent character to the interaction.

In order to quantify this correlation, we have coined the term "covalency quotient", which refers to the negative of the gradient of the line obtained by plotting the donor bond length against the interaction distance. We validated the covalency quotient against a number of other systems which have been more extensively studied, including halogen bonding, and both strong and weak hydrogen bonding. In all cases, the covalency quotient agreed with the expected origins of each interaction based on literature precedent. We also validated the covalency quotient against the computational energy decomposition analysis scheme SAPT for a number of model systems, which also showed excellent agreement. We believe the covalency quotient will prove to be a useful and generally applicable measure for σ-hole interactions, and we are currently working to extend the concept to the related phenomena of pnictogen and tetrel bonding, which remain comparatively underrepresented in the literature.

Finally, the experimental electron density in the co-crystals (determined through multipole refinement of high resolution x-ray diffraction data) was analysed within the QTAIM framework. The topology of the electron density in the vicinity of the Ch-bond was consistent with 3-centre–4-electron bonding, consistent with a strong covalent contribution.

These results will facilitate future work towards understanding the nature of intermolecular forces, and will aid in the design of materials and pharmaceuticals which exploit these forces.

Acknowledgement

We thank the Australian Research Council for Research Training Program (RTP) scholarships for TF and SB, and for a LIEF grant which supports the x-ray diffraction facility (LE170100065).

Supporting Information Available

Details of computational and analytical methods used in this work are available as supporting information, including synthetic methods and crystallographic data collection and refinement details. Supplementary figures S1-S10 and tables S1-S6 are also available. Crystallographic information for the structures reported have been submitted to the Cambridge Structural Database with codes 2257793–2257822 and 2268525–2268530.

References

(1) Vogel, L.; Wonner, P.; Huber, S. M. Chalcogen Bonding: An Overview. *Angewandte Chemie International Edition* **2019**, *58*, 1880–1891.

(2) Tarannam, N.; Shukla, R.; Kozuch, S. Yet Another Perspective on Hole Interactions. *Physical Chemistry Chemical Physics* **2021**, *23*, 19948–19963.

(3) Beno, B. R.; Yeung, K. S.; Bartberger, M. D.; Pennington, L. D.; Meanwell, N. A. A Survey of

the Role of Noncovalent Sulfur Interactions in Drug Design. *Journal of Medicinal Chemistry* **2015**, *58*, 4383–4438.

(4) Clark, T.; Hennemann, M.; Murray, J. S.; Politzer, P. Halogen bonding: the σ-hole. *Journal of Molecular Modeling* **2007**, *13*, 291–296.

(5) Hudson, B. M.; Nguyen, E.; Tantillo, D. J. The influence of intramolecular sulfur–lone pair interactions on small-molecule drug design and receptor binding. *Organic & Biomolecular Chemistry* **2016**, *14*, 3975–3980.

(6) Iwaoka, M.; Takemoto, S.; Tomoda, S. Statistical and theoretical investigations on the directionality of nonbonded S···O interactions. Implications for molecular design and protein engineering. *Journal of the American Chemical Society* **2002**, *124*, 10613–10620.

(7) Reid, R. C.; Yau, M. K.; Singh, R.; Lim, J.; Fairlie, D. P. Stereoelectronic effects dictate molecular conformation and biological function of heterocyclic amides. *Journal of the American Chemical Society* **2014**, *136*, 11914–11917.

(8) Biot, N.; Bonifazi, D. Programming Recognition Arrays through Double Chalcogen-Bonding Interactions. *Chemistry - A European Journal* **2018**, *24*, 5439–5443.

(9) Ho, P. C.; Wang, J. Z.; Meloni, F.; Vargas-Baca, I. Chalcogen Bonding in Materials Chemistry. *Coordination Chemistry Reviews* **2020**, *422*, 213464.

(10) Wang, W.; Zhu, H.; Feng, L.; Yu, Q.; Hao, J.; Zhu, R.; Wang, Y. Dual Chalcogen-Chalcogen Bonding Catalysis. *Journal of the American Chemical Society* **2020**, *142*, 3117–3124.

(11) Yan, W.; Zheng, M.; Xu, C.; Chen, F.-E. Harnessing Noncovalent Interaction of Chalcogen Bond in Organocatalysis: From the Catalyst Point of View. *Green Synthesis and Catalysis* **2021**, *2*, 329–336.

(12) Biot, N.; Bonifazi, D. Chalcogen-Bond Driven Molecular Recognition at Work. *Coordination Chemistry Reviews* **2020**, *413*, 213243.

(13) Lim, J. Y. C.; Marques, I.; Thompson, A. L.; Christensen, K. E.; Félix, V.; Beer, P. D. Chalcogen Bonding Macrocycles and [2]Rotaxanes for Anion Recognition. *Journal of the American Chemical Society* **2017**, *139*, 3122–3133.

(14) Garrett, G. E.; Carrera, E. I.; Seferos, D. S.; Taylor, M. S. Anion recognition by a bidentate chalcogen bond donor. *Chem. Commun.* **2016**, *52*, 9881–9884.

(15) Borissov, A.; Marques, I.; Lim, J. Y. C.; Félix, V.; Smith, M. D.; Beer, P. D. Anion recognition in water by charge-neutral halogen and chalcogen bonding foldamer receptors. *Journal of the American Chemical Society* **2019**, jacs.9b00148.

(16) Chen, L.; Xiang, J.; Zhao, Y.; Yan, Q. Reversible Self-Assembly of Supramolecular Vesicles and Nanofibers Driven by Chalcogen-Bonding Interactions. *Journal of the American Chemical Society* **2018**, *140*, 7079–7082.

(17) Ho, P. C.; Szydlowski, P.; Sinclair, J.; Elder, P. J. W.; Kübel, J.; Gendy, C.; Lee, L. M.; Jenkins, H.; Britten, J. F.; Morim, D. R.; Vargas-Baca, I. Supramolecular macrocycles reversibly assembled by Te. . . O chalcogen bonding. *Nature Communications* **2016**, *7*, 11299.

(18) Gleiter, R.; Werz, D. B.; Rausch, B. J. A world beyond hydrogen bonds? - Chalcogen-chalcogen interactions yielding tubular structures. *Chemistry - A European Journal* **2003**, *9*, 2676–2683.

(19) Garrett, G. E.; Gibson, G. L.; Straus, R. N.; Seferos, D. S.; Taylor, M. S. Chalcogen bonding in solution: Interactions of benzotelluradiazoles with anionic and uncharged Lewis bases. *Journal of the American Chemical Society* **2015**, *137*, 4126–4133.

(20) Bleiholder, C.; Werz, D. B.; Köppel, H.; Gleiter, R. Theoretical investigations on chalcogen-chalcogen interactions: What makes these nonbonded interactions bonding? *Journal of the American Chemical Society* **2006**, *128*, 2666–2674.

(21) Fellowes, T.; White, J. M. New insights into chalcogen bonding provided by co-crystal

structures of benzisoselenazolinone derivatives and nitrogen bases. *CrystEngComm* **2019**, *21*, 1539–1542.

(22) Pascoe, D. J.; Ling, K. B.; Cockroft, S. L. The Origin of Chalcogen-Bonding Interactions. *Journal of the American Chemical Society* **2017**, *139*, 15160–15167.

(23) Präsang, C.; Whitwood, A. C.; Bruce, D. W. Halogen-bonded cocrystals of 4-(N,N-dimethylamino)pyridine with fluorinated iodobenzenes. *Crystal Growth and Design* **2009**, *9*, 5319–5326.

(24) Sarwar, M. G.; Dragisic, B.; Salsberg, L. J.; Gouliaras, C.; Taylor, M. S. Thermodynamics of Halogen Bonding in Solution: Sub, Structural, and Solvent Effects. *Journal of the American Chemical Society* **2010**, *132*, 1646–1653.

(25) Beale, T. M.; Chudzinski, M. G.; Sarwar, M. G.; Taylor, M. S. Halogen bonding in solution: Thermodynamics and applications. *Chemical Society Reviews* **2013**, *42*, 1667–1680.

(26) Aakeröy, C. B.; Chopade, P. D.; Desper, J. Establishing a hierarchy of halogen bonding by engineering crystals without disorder. *Crystal Growth and Design* **2013**, *13*, 4145–4150.

(27) Goud, N. R.; Bolton, O.; Burgess, E. C.; Matzger, A. J. Unprecedented Size of the σ-Holes on 1,3,5-Triiodo-2,4,6-trinitrobenzene Begets Unprecedented Intermolecular Interactions. *Crystal Growth and Design* **2016**, *16*, 1765–1771.

(28) Stone, A. J. Are halogen bonded structures electrostatically driven? *Journal of the American Chemical Society* **2013**, *135*, 7005–7009.

(29) Parnham, M. J.; Sies, H. The early research and development of ebselen. *Biochemical Pharmacology* **2013**, *86*, 1248–1253.

(30) Shukla, R.; Claiser, N.; Souhassou, M.; Lecomte, C.; Balkrishna, S. J.; Kumar, S.; Chopra, D. Exploring the simultaneous σ-hole/π-hole bonding characteristics of a Br...π interaction in an

ebselen derivative via experimental and theoretical electron-density analysis. *IUCrJ* **2018**, *5*, 647–653.

(31) Fellowes, T.; Van Koeverden, M. M. P.; White, J. J. M. Thermal conversion of a pyridine solvate to a de-solvate facilitated by rearrangement of chalcogen bonds. The solvate and non-solvate structures of N-(2-nitro-4-(3-oxobenzo[d][1,2]selenazol-2(3H)-yl)phenyl)picolinamide. *CrystEngComm* **2020**, *22*, 4023–4029.

(32) Berthelot, M.; Laurence, C.; Safar, M.; Besseau, F. Hydrogen-bond basicity pKHB scale of six-membered aromatic N-heterocycles. *Journal of the Chemical Society, Perkin Transactions 2* **1998**, 283–290.

(33) Heinrich, M. R.; Klisa, H. S.; Mayr, H.; Steglich, W.; Zipse, H. Enhancing the Catalytic Activity of 4-(Dialkylamino)pyridines by Conformational Fixation. *Angewandte Chemie International Edition* **2003**, *42*, 4826–4828.

(34) Setter, C. J.; Whittaker, J. J.; Brock, A. J.; Arachchige, K. S. A.; McMurtrie, J. C.; Clegg, J. K.; Pfrunder, M. C. Straightening out Halogen Bonds. *CrystEngComm* **2020**, *22*, 1687–1690.

(35) **1CN** was also found in three distinct geometries, however this was due to the isolation of a dichloromethane solvate rather than polymorphism. We also note that the variation in bond lengths is much smaller than that seen in the electron rich derivatives.

(36) It is interesting to note that in all cases shorter N $\cdots$ Se distances for these derivatives are still associated with longer internal Se−N distances.

(37) Alhameedi, K.; Karton, A.; Jayatilaka, D.; Thomas, S. P. Bond Orders for Intermolecular Interactions in Crystals: Charge Transfer, Ionicity and the Effect on Intramolecular Bonds. *IUCrJ* **2018**, *5*, 635–646.

(38) Starbuck, J.; Norman, N. C.; Guy Orpen, A. Secondary Bonding as a Potential Design Element for Crystal Engineering. *New Journal of Chemistry* **1999**, *23*, 969–972.

(39) Aragoni, M. C.; Arca, M.; Devillanova, F. A.; Garau, A.; Isaia, F.; Lippolis, V.; Mancini, A. The nature of the chemical bond in linear three-body systems: From I 3- to mixed chalcogen/halogen and trichalcogen moieties. 2007.

(40) Puttreddy, R.; Jurček, O.; Bhowmik, S.; Mäkelä, T.; Rissanen, K. Very Strong -N–X+· · · –O–N+ Halogen Bonds. *Chemical Communications* **2016**, *52*, 2338–2341.

(41) Crabtree, R. H. Hypervalency, Secondary Bonding and Hydrogen Bonding: Siblings under the Skin. *Chemical Society Reviews* **2017**, *46*, 1720–1729.

(42) Riley, K. E.; Murray, J. S.; Fanfrlík, J.; Řezáč, J.; Solá, R. J.; Concha, M. C.; Ramos, F. M.; Politzer, P. Halogen bond tunability I: the effects of aromatic fluorine substitution on the strengths of halogen-bonding interactions involving chlorine, bromine, and iodine. *Journal of Molecular Modeling* **2011**, *17*, 3309–3318.

(43) Tsuzuki, S.; Wakisaka, A.; Ono, T.; Sonoda, T. Magnitude and Origin of the Attraction and Directionality of the Halogen Bonds of the Complexes of C6F5X and C6H5X (X=I, Br, Cl and F) with Pyridine. *Chemistry - A European Journal* **2012**, *18*, 951–960.

(44) Thirman, J.; Engelage, E.; Huber, S. M.; Head-Gordon, M. Characterizing the interplay of Pauli repulsion, electrostatics, dispersion and charge transfer in halogen bonding with energy decomposition analysis. *Physical Chemistry Chemical Physics* **2018**, *20*, 905–915.

(45) Ceccarelli, C.; Jeffrey, G. A.; Taylor, R. A survey of O-H· · · O hydrogen bond geometries determined by neutron diffraction. *Journal of Molecular Structure* **1981**, *70*, 255–271.

(46) The weak H-bonded system **GLOXIM11** is a self complementary dimer, so interaction energies are divided by two.

(47) Jeziorski, B.; Moszynski, R.; Szalewicz, K. Perturbation Theory Approach to Intermolecular Potential Energy Surfaces of van der Waals Complexes. *Chemical Reviews* **1994**, *94*, 1887–1930.

(48) Parker, T. M.; Burns, L. A.; Parrish, R. M.; Ryno, A. G.; Sherrill, C. D. Levels of symmetry adapted perturbation theory (SAPT). I. Efficiency and performance for interaction energies. *The Journal of Chemical Physics* **2014**, *140*, 094106.

(49) Stone, A. J.; Misquitta, A. J. Charge-transfer in Symmetry-Adapted Perturbation Theory. *Chemical Physics Letters* **2009**, *473*, 201–205.

(50) Weinhold, F.; Landis, C. R. *Discovering Chemistry with Natural Bond Orbitals*; John Wiley & Sons, Inc., 2012.

(51) Reed, A. E.; Curtiss, L. A.; Weinhold, F. Intermolecular Interactions from a Natural Bond Orbital, Donor—Acceptor Viewpoint. *Chemical Reviews* **1988**, *88*, 899–926.

(52) Bader, R. F. A Quantum Theory of Molecular Structure and Its Applications. *Chemical Reviews* **1991**, *91*, 893–928.

(53) Thomas, S. P.; Dikundwar, A. G.; Sarkar, S.; Pavan, M. S.; Pal, R.; Hathwar, V. R.; Row, T. N. G. The Relevance of Experimental Charge Density Analysis in Unraveling Noncovalent Interactions in Molecular Crystals. *Molecules* **2022**, *27*, 3690.

(54) Thomas, S. P.; Satheeshkumar, K.; Mugesh, G.; Guru Row, T. N. Unusually Short Chalcogen Bonds Involving Organoselenium: Insights into the Se–N Bond Cleavage Mechanism of the Antioxidant Ebselen and Analogues. *Chemistry – A European Journal* **2015**, *21*, 6793–6800.

(55) Xu, R.; Fellowes, T.; White, J. M. High-Resolution Structural Study on Pyridin-3-Yl Ebselen and Its *N* -Methylated Tosylate and Iodide Derivatives. *Acta Crystallographica Section C Structural Chemistry* **2023**, *79*, 43–51.

(56) Molina, J.; Dobado, J. A. The three-center-four-electron (3c-4e) bond nature revisited. An atoms-in-molecules theory (AIM) and ELF study. *Theoretical Chemistry Accounts* **2001**, *105*, 328–337.

For Table of Contents use only

Hammett Structural Relationships Revealed in Chalcogen Bonded Co-crystals of Electron Rich Pyridines with 4′-Substituted Ebselen Derivatives

Thomas Fellowes, Eric Lee, Jennifer Tran, Ruyi Xu, Alec Barber, Samuel C. Brydon, Jack K. Clegg, and Jonathan M. White

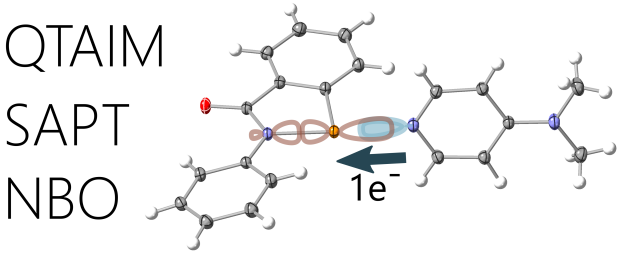

Detailed analysis of a series of crystal structures containing chalcogen bonds shows that there is a significant covalent component to the interaction, which is attributed to a n $\rightarrow \sigma^{\star}$ delocalisation. This finding is supported by computational energy decomposition analysis, and also by modelling the experimental electron density in several crystals via multipole refinement.